

CSSDF-Net: Safe Motion Planning Based on Neural Implicit Representations of Configuration Space Distance Field

Haohua Chen^{1,*}, Yixuan Zhou^{1,*}, Yifan Zhou¹ and Hesheng Wang^{1,†}

Abstract—High-dimensional manipulator operation in unstructured environments requires a differentiable, scene-agnostic distance query mechanism to guide safe motion generation. Existing geometric collision checkers are typically non-differentiable, while workspace-based implicit distance models are hindered by the highly nonlinear workspace–configuration mapping and often suffer from poor convergence; moreover, self-collision and environment collision are commonly handled as separate constraints. We propose Configuration-Space Signed Distance Field-Net (CSSDF-Net), which learns a continuous signed distance field directly in configuration space to provide joint-space distance and gradient queries under a unified geometric notion of safety. To enable zero-shot generalization without environment-specific retraining, we introduce a spatial-hashing-based data generation pipeline that encodes robot-centric geometric priors and supports efficient retrieval of risk configurations for arbitrary obstacle point sets. The learned distance field is integrated into safety-constrained trajectory optimization and receding-horizon MPC, enabling both offline planning and online reactive avoidance. Experiments on a planar arm and a 7-DoF manipulator demonstrate stable gradients, effective collision avoidance in static and dynamic scenes, and practical inference latency for large-scale point-cloud queries, supporting deployment in previously unseen environments.

I. INTRODUCTION

As robots increasingly transition from controlled industrial settings to highly complex and unstructured real-world environments, the development of robust collision avoidance mechanisms has become increasingly essential.

To generate feasible trajectories that simultaneously satisfy safety and smoothness constraints, nonlinear optimization-based backend trajectory optimization algorithms are typically employed. The core of these methods lies in the gradient-guided escaping from unsafe region. However, in practical, the accurate computation of distance gradients for complex shapes with compact geometric representations (e.g., convex hulls) poses significant challenges, particularly when handling dynamic obstacles that require complex mathematical derivations.

Recently, implicit modeling strategies becomes a main solution to obtain differentiable, and high-fidelity representations of complex geometric boundaries. Specifically, distance proxy models can be constructed to represent the relationship between the robot and collision objects. However, due to the highly nonlinear mapping between the workspace and the configuration space (C-space), such methods are susceptible to local minima for manipulators. This has motivated the

direct modeling of distance fields in C-space, thereby avoiding the inherent limitations of workspace-based methods caused by inverse-kinematics projections. However, existing approaches in C-Space still face two major challenges:

Challenge 1: How to achieve a scenario-agnostic neural implicit representation without retraining across different environments? A cascaded frameworks that map a pre-trained workspace SDF to C-space [1] may complicates the pipeline by introducing additional pre-training stages, and exacerbates error accumulation across modules, ultimately degrading robustness and generalization.

Challenge 2: How to unify self-collision and environment collision into a single geometric notion of safety? Prior work often models these constraints separately—for example, assuming self-collision is implicitly avoided within manufacturer-defined joint limits, or training solely for self-collision.

To solve these two challenges, we design Configuration-Space Signed Distance Field-Net (CSSDF-Net), a deep neural network (DNN) to provide continuous distance/gradient query directly in C-space. Our core contributions are as follows:

- CSSDF-Net is introduced to model a continuous, differentiable signed distance field directly in configuration space, providing a unified geometric notion of safety for both self-collision and environment collision.
- A spatial-hashing data generation pipeline is developed to train a scene-agnostic model, removing the need for environment-specific retraining and cascaded SDF mappings.
- The learned distance field and gradients are integrated into vision-guided motion planning and trajectory optimization, enabling real-time collision checking and safe motion generation in static and dynamic scenes.

II. RELATED WORKS

Current researches on robot collision avoidance can be split into two main branches, free space approximation and distance field modeling.

A. Free Space Approximation

Early studies, such as sampling-based planning algorithms, a series of methods developed from probabilistic roadmaps (PRM [2]) and rapidly exploring random trees (RRT [3]), construct a roadmap or a tree by randomly sampling collision-free configurations via a binary feasibility test and then search for a path; in essence, this amounts to an approximate construction of the topological structure

¹ Authors are with the IRMV Lab, Department of Automation, Shanghai Jiao Tong University, Shanghai 200240, China.

of the free space. Similarly, this approximation paradigm has been widely adopted in mobile robotics, particularly in autonomous driving and unmanned aerial vehicles (UAVs). In these domains, the approach is often referred to as a safe flight corridor, where simple structures such as spheres and cubes are used in the task space [4]–[6] to construct a collection of collision-free regions as the feasible set, and this idea has been further extended to more general convex polytopes [7], [8]. Although the above methods are difficult to apply directly to high-dimensional problems due to the “curse of dimensionality,” techniques such as mathematical mappings can be leveraged to transfer them to the configuration space [9]–[11].

B. Distance Field Modeling

Distance modeling methods can be categorized into two types: explicit and implicit. Explicit computation often employs geometric intersection algorithms such as GJK [12]. However, GJK is not mathematically differentiable and typically provides only a binary collision verdict and a distance value in FCL [13], PyBullet [14], lacking continuous information to guide downstream application. Consequently, implicit approaches that fit Euclidian Signed Distance Field (ESDF) with neural networks have emerged and have been successfully applied to scenarios such as autonomous driving and UAVs [15], [16].

For high-dimensional problems, the nonlinear mapping between task space and configuration space makes task-space distance fields difficult to use. Recent studies suggest that modeling collisions directly in the robot configuration space [17] effectively overcomes inherent limitations of kinematics-based collision checking, such as singularities and local convergence issues. For static environments or self-collision scenarios, existing methods primarily sample the robot joint space and employ machine-learning techniques to represent collision boundaries [18]. For dynamic environments, configuration-space distance field (CDF) [19] models the robot as a particle system where obstacles form explicit topological holes in the configuration space. The CDF approach is highly compatible and scalable, seamlessly integrating with modern geometric motion-planning frameworks such as Riemannian motion policies [20], geometric fabrics [21].

III. METHODOLOGY

A. Problem Formulation

Consider a robot with m joints, of which d are actively actuated. The remaining $m - d$ joints are passive or fixed. Since motion involves only the active joints, the robot configuration is uniquely defined by the vector $\mathbf{q} \in \mathbb{R}^d$. The corresponding topological space $\mathcal{Q} \subset \mathbb{R}^d$ is termed the configuration space.

Assume the robot comprises $k_r > m$ rigid links, each with $h > 0$ attached collision bodies, denoted by $\mathcal{C}_i = \{c_i^1, \dots, c_i^h\}$. A generalized self-collision distance function incorporating

both link-to-link collisions and joint limits is defined as:

$$d_s(\mathbf{q}) = \begin{cases} \min_{\mathbf{q}_c \in \mathcal{Q}^c} \|\mathbf{q} - \mathbf{q}_c\|_2, & \mathbf{q} \in \mathcal{Q}^s, \\ -\min_{\mathbf{q}_f \in \mathcal{Q}^s} \|\mathbf{q} - \mathbf{q}_f\|_2, & \mathbf{q} \in \mathcal{Q}^c. \end{cases} \quad (1)$$

where \mathcal{Q}^s and \mathcal{Q}^c denote the safe and self-collision configuration sets, respectively.

To establish a single geometric notion of safety, we treat pure self-collision as a special case of external collision where the obstacle point lies outside the reachable workspace. Suppose the workspace contains $g > 0$ static or dynamic obstacles, denoted by $\mathcal{O} = \{O_1, \dots, O_g\}$. For an arbitrary point $\mathbf{p} \in \mathbb{R}^3$ (either on an obstacle or virtual for self-collision), the signed distance function is given by:

$$d_c(\mathbf{p}, \mathbf{q}) = \begin{cases} \min_{\mathbf{q}_c \in \mathcal{Q}_c^p} \|\mathbf{q} - \mathbf{q}_c\|_2, & \mathbf{q} \notin \mathcal{Q}_c^p, \\ -\min_{\mathbf{q}_f \notin \mathcal{Q}_c^p} \|\mathbf{q} - \mathbf{q}_f\|_2, & \mathbf{q} \in \mathcal{Q}_c^p. \end{cases} \quad (2)$$

where \mathcal{Q}_c^p represents the set of configurations colliding with point \mathbf{p} . For self-collision, \mathbf{p} is treated as a virtual point with $\mathcal{Q}_c^p \equiv \mathcal{Q}^c$.

Combining Eq. 1 and Eq. 2 yields the composite signed distance function for a single point \mathbf{p} :

$$d(\mathbf{p}, \mathbf{q}) = \begin{cases} \max(d_s(\mathbf{q}), d_c(\mathbf{p}, \mathbf{q})), & d_s(\mathbf{q}) < 0 \wedge d_c(\mathbf{p}, \mathbf{q}) < 0, \\ \min(d_s(\mathbf{q}), d_c(\mathbf{p}, \mathbf{q})), & \text{otherwise.} \end{cases} \quad (3)$$

The max operation ensures the most critical collision source dominates when both self-collision and external collision occur simultaneously, while min selects the nearest safety boundary otherwise.

Extending this to k_o discrete obstacle points $\mathcal{C} = \{\mathbf{p}_1, \dots, \mathbf{p}_{k_o}\}$ in the workspace, the composite signed distance function is expressed as:

$$d(\mathcal{C}, \mathbf{q}) = \begin{cases} \max_{i=1, \dots, k_o} d(\mathbf{p}_i, \mathbf{q}), & \forall d(\mathbf{p}_i, \mathbf{q}) < 0, \\ \min_{i=1, \dots, k_o} d(\mathbf{p}_i, \mathbf{q}), & \text{otherwise.} \end{cases} \quad (4)$$

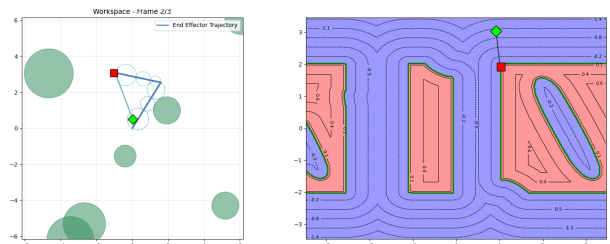


Fig. 1: Gradient-guided escape in configuration space. Unlike Euclidean space methods requiring iterative projections through inverse kinematics (multi-step, curved paths), our C-space SDF enables direct single-step escape along the configuration gradient.

The signed distance function exhibits the following linear homogeneity properties:

$$\|\nabla_{\mathbf{q}} d(\mathbf{p}, \mathbf{q})\|_2 = 1, \mathbf{q}_{\text{boundary}} = \mathbf{q}_1 - d(\mathbf{p}, \mathbf{q}_1) \nabla_{\mathbf{q}} d(\mathbf{p}, \mathbf{q}_1), \quad (5)$$

where the first property indicates unit Lipschitz continuity, and the second provides an explicit expression for reaching the collision boundary along the gradient direction.

Fig. 1 illustrates the key advantage of configuration-space representation: the initial robot configuration (green end-effector) inside an obstacle escapes to a safe region (red end-effector) along the shortest path in \mathcal{Q} , requiring only a single linear iteration. This contrasts with workspace-based methods that require multiple inverse-kinematics projections, resulting in curved, inefficient escape trajectories.

B. CSSDF-Net Architecture

1) *Network Structure*: CSSDF-Net takes concatenated input $\mathbf{x} = [\mathbf{q}; \mathbf{p}] \in \mathbb{R}^{n+3}$, where $\mathbf{q} \in \mathbb{R}^n$ is the configuration vector and $\mathbf{p} \in \mathbb{R}^3$ is the obstacle point (or virtual point for self-collision). The network employs a 5-layer MLP backbone (216 neurons per layer) with identity residual connections, utilizing ReLU activations, batch normalization, positional encoding, and dropout ($p = 0.2$). To balance the distribution of safe and collision data, inputs are min-max normalized to $[-1, 1]$ using extended joint limits $[\min(-\pi, \mathbf{q}_{\min}), \max(\pi, \mathbf{q}_{\max})]$. The corresponding inverse transform of the gradient is applied via the chain rule during backpropagation to maintain optimization stability. The model is trained using the AdamW optimizer [22] with a ReduceLRonPlateau scheduler.

The network is supervised by a composite loss function $\mathcal{L} = 5\mathcal{L}_{\text{dist}} + 0.1\mathcal{L}_{\text{eikonal}} + 0.2\mathcal{L}_{\text{dir}}$, comprising three terms:

1) **MSE Regression Loss** ($\mathcal{L}_{\text{dist}}$) minimizes the error between the predicted $\hat{d}(\mathbf{x}_i)$ and ground-truth $d(\mathbf{x}_i)$ CSSDF values:

$$\mathcal{L}_{\text{dist}} = \frac{1}{b} \sum_{i=0}^{b-1} (\hat{d}(\mathbf{x}_i) - d(\mathbf{x}_i))^2. \quad (6)$$

2) **Eikonal Regularization Loss** ($\mathcal{L}_{\text{eikonal}}$) enforces the unit-gradient geometric property ($\|\nabla d\| = 1$) of the SDF:

$$\mathcal{L}_{\text{eikonal}} = \frac{1}{b} \sum_{i=0}^{b-1} (\|\nabla_{\mathbf{q}} d(\mathbf{x}_i)\|_2 - 1)^2. \quad (7)$$

3) **Gradient Direction Consistency Loss** (\mathcal{L}_{dir}) aligns the predicted and true gradient directions via cosine similarity to ensure reliable downstream motion planning:

$$\mathcal{L}_{\text{dir}} = \frac{1}{b} \sum_{i=0}^{b-1} \left(1 - \frac{\nabla_{\mathbf{q}} \hat{d}(\mathbf{x}_i)^\top \nabla_{\mathbf{q}} d(\mathbf{x}_i)}{\|\nabla_{\mathbf{q}} \hat{d}(\mathbf{x}_i)\| \|\nabla_{\mathbf{q}} d(\mathbf{x}_i)\|} \right)^2. \quad (8)$$

C. Dataset Construction

The dataset generation pipeline produces unified (\mathbf{q}, \mathbf{p}) tuples for both self-collision and external collision scenarios.

1) *Self-Collision Dataset Construction*: The configuration space $\mathcal{Q} \subset \mathbb{R}^n$ is uniformly sampled to generate a base configuration set $Q_{\text{base}} \in \mathbb{R}^{N \times n}$, where N is the sample size and n denotes the degrees of freedom (DoF). An FCL-based collision checker $f_{\text{col}}: \mathcal{Q} \rightarrow \{0, 1\}$ labels each configuration as safe (0) or in-collision (1). To mitigate the class imbalance inherent in random sampling, an adaptive strategy is introduced: if the ratio of collision to free samples ($p_{\text{col}}/p_{\text{free}}$)

exceeds a threshold $\tau = 1.25$, neighborhood perturbation augmentation is applied.

To capture the complex, high-dimensional decision boundaries in the joint space, a boundary mining mechanism employing Hierarchical Navigable Small World (HNSW) graphs [23] is utilized. HNSW provides logarithmic-complexity nearest-neighbor search suitable for high-dimensional boundary extraction. By maintaining separate search trees for collision and free samples, the nearest neighbor \mathbf{q}_i^{nn} of a configuration \mathbf{q}_i in the opposing tree is queried. A bisection search between \mathbf{q}_i and \mathbf{q}_i^{nn} then isolates the precise decision boundary point. Upon convergence, the new boundary sample $\mathbf{q}_{\text{boundary}}$ is added to its respective tree.

The ground-truth distance and gradient are then obtained for any point \mathbf{q}_i :

$$d(\mathbf{q}_i) = \|\mathbf{q}_i - \mathbf{q}_{\text{boundary}}\|, \quad \nabla d_{\mathbf{q}} = \frac{1}{d}(\mathbf{q}_i - \mathbf{q}_{\text{boundary}}). \quad (9)$$

The final dataset comprises random, perturbed, and boundary samples, formulated as tuples $(Q, \text{value}, \text{labels}, \nabla)$. Here, $Q \in \mathbb{R}^{b \times (n+3)}$ denotes the concatenated configuration-obstacle vector, $\text{value} \in \mathbb{R}^b$ is the signed distance, $\text{labels} \in \{0, 1\}^b$ is the binary collision label, and $\nabla \in \mathbb{R}^{b \times n}$ is the spatial gradient. To ensure that the self-collision notion could be visited correctly with no obstacles (outside the workspace), workspace coordinates are sampled from an extended space \mathcal{W}_{ext} rather than the strictly reachable space $\mathcal{W}_{\text{reachable}}$.

2) *External Collision Dataset Construction*: To achieve scene-agnostic neural implicit representation without environment-specific retraining, a configuration-to-workspace mapping is established that decouples robot-specific geometric priors from scene-dependent obstacle information. The core innovation lies in a spatial hashing mechanism that enables constant-time retrieval of risk configurations for arbitrary obstacle layouts.

Spatial Hashing for Configuration-Voxel Association: The robot geometry is approximated as sphere clusters via `SpherizedURDFGenerator`¹, yielding occupied region $\mathcal{O}(\mathbf{q}) = \bigcup_{i=1}^m B(\mathbf{c}_i(\mathbf{q}), r_i(\mathbf{q}))$ for configuration \mathbf{q} . The workspace $\mathcal{W} \subset \mathbb{R}^3$ is discretized with resolution Δx , and a spatial hash function $h: \mathbb{R}^3 \rightarrow \mathbb{Z}^3$ maps continuous positions to voxel indices: $h(\mathbf{p}) = \lfloor (\mathbf{p} - \mathbf{w}_{\min}) / \Delta x \rfloor$.

For each collision sphere $B(\mathbf{c}, r)$, the influenced voxel set $\mathcal{S}(B)$ is computed, establishing the grid-configuration mapping:

$$\mathcal{M}(g) = \{\mathbf{q} \in \mathcal{Q} \mid \exists B \in \mathcal{O}(\mathbf{q}), g \in \mathcal{S}(B) \wedge B \cap g \neq \emptyset\}. \quad (10)$$

Algorithm 1 constructs \mathcal{M} offline via parallel computation. This mapping is computed *once* during training and enables constant-time retrieval of all configurations potentially occupying any voxel g at data generation.

Zero-Shot capabilities for Novel Environments. Crucially, \mathcal{M} encodes robot-centric geometric priors that are independent of specific obstacle placements. The spatial

¹<https://github.com/IRMV-Manipulation-Group/SpherizedURDFGenerator>

Algorithm 1: Parallel Spatial Hashing Construction

Data: Configurations \mathcal{Q} , kinematic mapping

$$f: \mathcal{C} \rightarrow 2^{\mathcal{B}}$$

Result: Mapping $\mathcal{M}: \mathcal{G} \rightarrow 2^{\mathcal{Q}}$

```
1 Initialize  $\mathcal{M} \leftarrow \emptyset$ ;  
2 foreach  $q \in \mathcal{Q}$  parallel do  
3    $\mathcal{B} \leftarrow f(q)$ ;  
4   foreach  $B(c, r) \in \mathcal{B}$  do  
5      $\mathcal{I}(B) \leftarrow$  compute influence region;  
6     foreach  $g \in \mathcal{I}(B)$  do  
7       if  $B \cap g \neq \emptyset$  then  
8          $\mathcal{M}(g) \leftarrow \mathcal{M}(g) \cup \{q\}$   
9       end  
10    end  
11  end  
12 end  
13 return  $\mathcal{M}$ ;
```

hashing mechanism discretizes the workspace into voxels solely to determine the key-problem: how to obtain the zero-level-set of obstacle point p in configuration space. This problem was treated as a nonlinear-projection problem in [1] using a pre-trained ESDF model. For data generation, given point p , the voxel g is found and queried in \mathcal{M} to obtain \mathcal{Q}_c^p in (2). Similar to (9), ground truth for external collision is produced.

Notice that, although the input data is discretized, the trained MLP learns a continuous representation of this space, with its intrinsic function approximation capability providing smooth interpolation across the entire workspace. When deployed in novel environments, incoming obstacle point clouds are simply transformed into the robot-centric coordinate frame and fed directly as continuous coordinates $p \in \mathbb{R}^3$ to the network. No voxel discretization is required at inference time—the network naturally generalizes to arbitrary obstacle positions within its learned spatial bounds, effectively activating the corresponding geometric memories encoded during training. For dynamic scenes, updated sensor observations are transformed and queried at each timestep without model retraining.

D. Motion Planning and Control Integrating CSSDF-Net

1) *Safe MPC for Dynamic Environments:* To demonstrate the capability of handling dynamic environments, the differentiable distance field learned by CSSDF-Net is integrated into a Model Predictive Control (MPC) framework. By formulating a safety-constrained receding horizon optimization problem, this approach ensures that the system can reactively stay within the safe configuration space while satisfying kinematic limits during trajectory tracking.

Consider an n -DOF manipulator system, whose discrete-time state function can be expressed as a single-integrator model: $\mathbf{q}_{k+1} = \mathbf{A}\mathbf{q}_k + \mathbf{B}\mathbf{u}_k$, where $\mathbf{q}_k \in \mathbb{R}^n$ is the joint configuration at time step k , $\mathbf{u}_k \in \mathbb{R}^n$ is the control input (joint velocity), $\mathbf{A} = \mathbf{I}_n$ is the state transition matrix, $\mathbf{B} = \Delta t \cdot \mathbf{I}_n$ is the control input matrix, and Δt is the sampling

period. To maintain the safety margin $\phi(\mathbf{q}_k) \geq \gamma$, the following linearized inequality constraint must be satisfied: $\nabla\phi(\mathbf{q}_k)^\top(\mathbf{q}_{k+1} - \mathbf{q}_k) \geq \Delta t(\gamma - \phi(\mathbf{q}_k))$. Therefore, we design a safe MPC controller to solve the following constrained optimization problem over the prediction horizon H :

$$\begin{aligned} \min_{\mathbf{u}} \quad & \sum_{k=0}^{H-1} (\|\mathbf{q}_k - \hat{\mathbf{q}}_k\|_{\mathbf{Q}}^2 + \|\mathbf{u}_k\|_{\mathbf{R}}^2), \\ \text{s.t.} \quad & \mathbf{q}_{k+1} = \mathbf{A}\mathbf{q}_k + \mathbf{B}\mathbf{u}_k, \quad k = 0, \dots, H-1, \\ & \mathbf{q}_{\min} \leq \mathbf{q}_k \leq \mathbf{q}_{\max}, \quad k = 1, \dots, H, \\ & \mathbf{u}_{\min} \leq \mathbf{u}_k \leq \mathbf{u}_{\max}, \quad k = 0, \dots, H-1, \\ & \nabla\phi(\mathbf{q}_k)^\top(\mathbf{q}_{k+1} - \mathbf{q}_k) \geq (\gamma - \phi(\mathbf{q}_k))\Delta t, \quad k = 1, \dots, H-1, \end{aligned} \quad (11)$$

Here, $\hat{\mathbf{q}}_k$ denotes the reference point on the target trajectory, \mathbf{Q} and \mathbf{R} are positive definite weight matrices, and $\gamma > 0$ represents the preset safety margin threshold. We utilize an efficient Quadratic Programming (QP) solver, such as OSQP, to solve the optimization problem in (11) in real time.

2) *Safety-Constrained Trajectory Optimization for Offline Planning:* To evaluate the offline processing performance, we formulate a safety-constrained trajectory optimization framework based on CSSDF-Net. The core of this framework lies in the seamless integration of the learned distance field and its gradient information into the backend optimization. This enables efficient offline generation of safe trajectories by rigorously evaluating safety constraints, encompassing both external and self-collisions. The objective function for the spatiotemporal trajectory optimization is formulated as:

$$\begin{aligned} \min_{\mathbf{q}, T_i} \quad & \sum_{i=0}^{n-1} \left(\lambda_s \frac{T_i}{3} \text{tr}(\mathbf{m}_j^T \mathbf{K}_2 \mathbf{m}_j) + \lambda_t T_i \right. \\ & \left. + \lambda_p \|T_i - T_{i-1}\|^2 + \lambda_q \|\mathbf{q}_{i+1} - \mathbf{q}_i\| \right) + \lambda_\phi \mathbf{M}_s(\mathbf{q}), \\ \text{s.t.} \quad & \mathbf{q}_i \in [\mathbf{q}_{\min}, \mathbf{q}_{\max}], \quad \mathbf{m}_i \in [\hat{\mathbf{q}}_{\min}, \hat{\mathbf{q}}_{\max}], \\ & \frac{\mathbf{q}_{i+1} - \mathbf{q}_i}{T_i} - \frac{T_i}{3} \mathbf{m}_i - \frac{T_i}{6} \mathbf{m}_{i+1} \in [\hat{\mathbf{q}}_{\min}, \hat{\mathbf{q}}_{\max}], \\ & \hat{\mathbf{q}}_0 = \mathbf{v}_s, \hat{\mathbf{q}}_n = \mathbf{v}_e, T_i > 0 \end{aligned} \quad (12)$$

where $\mathbf{K}_2 = \begin{bmatrix} 1 & 1 \\ 0 & 1 \end{bmatrix}$ is the weight matrix, $\mathbf{m}_j = [\mathbf{m}_j^T, \mathbf{m}_{j+1}^T]^T$ represents the concatenated vector of accelerations at adjacent control points, $\mathbf{q} = [\mathbf{q}_0, \dots, \mathbf{q}_N]^T$ is the sequence of spline control points, and $\mathbf{T} = [T_0, \dots, T_N]$ is the vector of time allocation parameters.

In this framework, the safety penalty term \mathbf{M}_s utilizes a continuously differentiable piecewise exponential function:

$$\mathbf{M}_s(\mathbf{q}) = \sum_{k=0}^{n-1} \begin{cases} \exp\left(-\frac{\phi(\mathbf{q}_k)}{d_0}\right) - 1, & \phi(\mathbf{q}_k) < 0 \\ \exp(-\alpha(\phi(\mathbf{q}_k) + d_0)), & \phi(\mathbf{q}_k) \geq 0 \end{cases} \quad (13)$$

where $\phi(\cdot)$ denotes the configuration space signed distance queried directly from CSSDF-Net.

It is worth emphasizing that because CSSDF-Net provides an accurate and continuous characterization of the safety boundary, this offline method can aggressively minimize the trajectory length by incorporating the term $\|\mathbf{q}_{i+1} - \mathbf{q}_i\|$

into the objective function while strictly guaranteeing safety. This capability distinguishes our approach from classic optimization frameworks that often struggle to balance path optimality with rigorous collision avoidance.

IV. EXPERIMENTS AND RESULTS

A. 2D Experiments

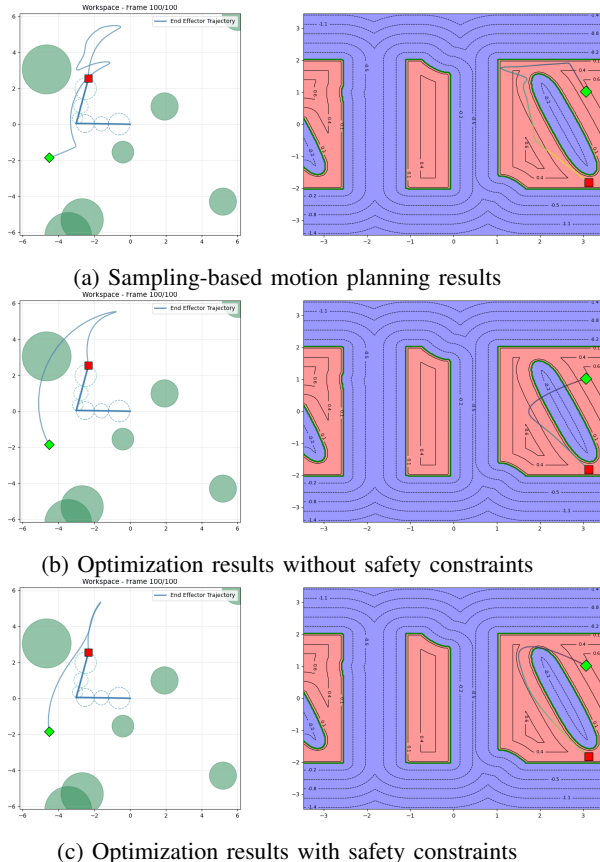


Fig. 2: Comparative analysis of trajectory optimization with safety constraints.

To provide an intuitive validation of CSSDF-Net and its gradient-guided safety constraints, we first conduct experiments with a 2-DoF planar manipulator. Its configuration space is $\mathcal{Q} \subset \mathbb{R}^2$ with joint angles $[q_1, q_2]^T \in [-\pi, \pi]^2$, and the workspace $\mathcal{W} \subset \mathbb{R}^2$ is a 12×12 m² region containing circular obstacles.

1) *Static Environment*: As shown in Fig. 2, sampling-based planners generate collision-free solutions but often produce jagged trajectories (Fig. 2a). In contrast, unconstrained trajectory optimization yields smooth paths but can penetrate obstacles due to the lack of a safety term (Fig. 2b). By integrating CSSDF-Net queries $\phi(\mathbf{q})$ and $\nabla\phi(\mathbf{q})$ into the optimization, the resulting trajectories are both smooth and collision-free (Fig. 2c), indicating that the learned C-space SDF provides usable gradients for escaping unsafe regions and converging to safe optima.

Table I reports quantitative results in terms of Collision Risk (CR), Trajectory Length (TL), and Average Time (AT).

The CSSDF-Net-guided safe optimization achieves 0% CR with shorter trajectories than pure sampling, at the cost of higher computation time (130.48 ms). This trade-off reflects the additional safety evaluations while supporting our goal of enabling safety-critical, gradient-based trajectory optimization.

TABLE I: Comparative performance of trajectory planning for the planar manipulator

Methods	Metrics		
	CR(%)↓	TL↓	AT (ms)↓
Sampling	0.	8.359	1.702
Sampling + Non-safe optimization	6.100	5.793	3.216
Sampling + Safe optimization	0.	5.928	130.48

2) *Dynamic Environment*: We further evaluate the method in a dynamic environment with a 0.3 m rectangular obstacle moving leftward at a constant speed. At each control cycle, CSSDF-Net provides $\phi(\mathbf{q})$ and $\nabla\phi(\mathbf{q})$ for the observed obstacle points, which are used in the receding-horizon controller (Eq. (11)) to enforce the linearized safety constraint.

Figure 3 illustrates the avoidance process. When the obstacle enters the affected region (Fig. 3a), the controller promptly generates a safe deviation. After the obstacle leaves (Fig. 3b), the manipulator smoothly returns to its nominal motion and reaches the goal (Fig. 3c), demonstrating that the learned distance gradients remain stable for online reactive control.

B. Ablation Studies

Ablation experiments were performed on an NVIDIA RTX 3060 GPU using 1×10^4 samples with an 8:2 train-validation split. To evaluate reliability near the decision boundary, we define the False Positive Rate (FPR) as:

$$\text{FPR} = \frac{\sum_{i=1}^{N_B} \mathbb{I}(\hat{d}(\mathbf{x}_i) < 0 \cap d(\mathbf{x}_i) > 0)}{N_B} \times 100\% \quad (14)$$

where N_B denotes the number of samples within 0.05 rad of the collision boundary and $\mathbb{I}(\cdot)$ is the indicator function.

1) *Dataset Construction Strategy*: The complete strategy increases the Boundary Sample Ratio (BSR) to 35.5656%, whereas uniform sampling yields a 0% BSR, indicating insufficient coverage of boundary regions. This improvement is accompanied by the lowest MAE and a near-balanced class ratio (51.7351%), supporting the effectiveness of boundary mining for learning accurate C-space safety boundaries.

2) *Loss Functions*: Training with only distance loss yields low gradient similarity and a high FPR (15.45%), which is undesirable for gradient-based planning and MPC linearization. Adding the direction loss improves gradient similarity and reduces FPR, while the eikonal (magnitude) term further stabilizes gradient behavior. Overall, the complete composite loss achieves the lowest MAE and reduces FPR to 8.42%, providing more reliable gradients for downstream optimization.

TABLE II: Comprehensive Ablation Results on CSSDF-Net Components

Configuration	Primary Metrics		Secondary Specific Metrics			
	MAE (rad) ↓	Grad. Sim. ↑	FPR (%) ↓	Latency (μ s) ↓	BSR (%) ↑	Class Ratio (%)
Data Construction Strategy						
Uniform Sampling	0.1256	0.8536	–	–	0.0000	86.9000
Class-Balanced Sampling	0.1029	0.8698	–	–	0.0117	50.8505
Complete Strategy	0.0754	0.8762	–	–	35.5656	51.7351
Loss Function						
Only Distance Loss	0.1417	0.6645	15.4535	–	–	–
Distance + Magnitude Loss	0.1369	0.6654	16.1909	–	–	–
Distance + Direction Loss	0.1231	0.7517	11.7244	–	–	–
Complete Loss	0.0754	0.8536	8.4167	–	–	–

Note: MAE = Distance Mean Absolute Error; Grad. Sim. = Gradient Direction Similarity;
FPR = Boundary False Positive Rate; BSR = Boundary Sample Ratio.

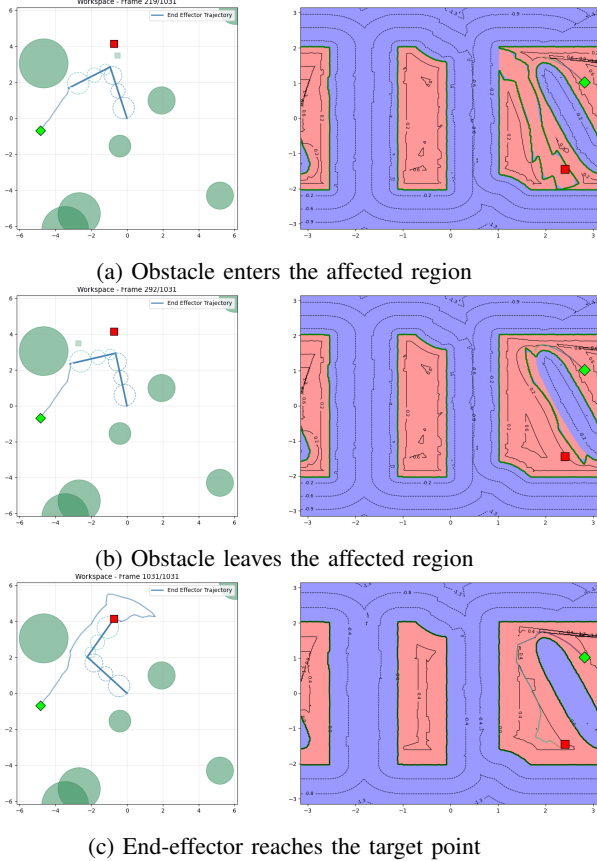


Fig. 3: Evolution of the dynamic obstacle avoidance process.

C. Real-World Manipulator Experiments

To validate scalability in higher-dimensional configuration spaces, we conducted experiments on a 7-DoF manipulator (Fig. 4). The workspace includes static obstacles and human-driven dynamic obstacles, evaluating both trajectory optimization and online avoidance.

1) *Real-Time Inference Performance*: Table III reports inference latency for distance and distance+gradient queries under different point-cloud sizes. GPU execution achieves millisecond-level latency for 10^2 – 10^4 points (e.g., 4.302 ms at 10^4 points for distance+gradient), enabling high-frequency replanning. CPU inference remains practical up to 10^3 points

(5.846 ms for distance+gradient), supporting real-time deployment under moderate sensing loads.

TABLE III: System inference performance for the 7-DoF manipulator

Computing Mode	Query Scale (Number of Points)					
	10^0	10^1	10^2	10^3	10^4	10^5
Dis (CPU)	0.302	0.367	0.633	2.431	28.721	286.053
Dis+Grad (CPU)	0.704	0.866	1.576	5.846	58.785	578.978
Dis (GPU)	1.185	1.102	1.107	1.174	2.118	22.193
Dis+Grad (GPU)	2.676	2.551	2.549	2.739	4.302	43.233

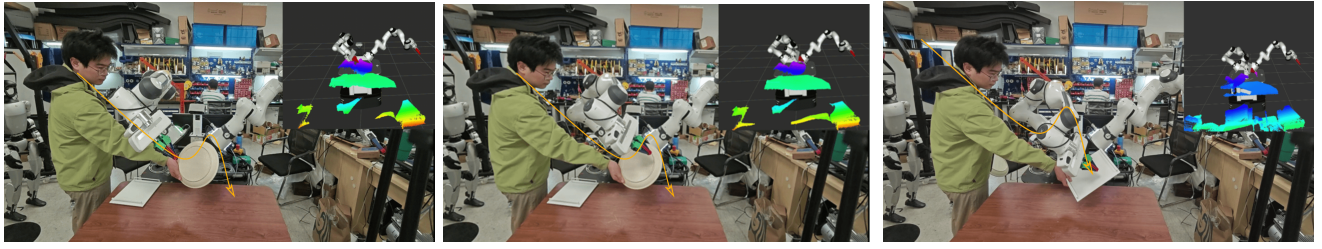
2) *Trajectory Optimization in Static Environments*: CSSDF-Net-guided safe optimization achieves low collision risk (0.561%) and significantly shorter trajectories (18.054 rad) compared to pure sampling (34.279 rad) (Table IV). Although safety constraints increase the computation time, the 171.117 ms latency is practical for offline planning.

3) *Experiments in Dynamic Environments*: We integrated CSSDF-Net into the MPC controller to evaluate real-time avoidance using dynamic point clouds updated at 100 Hz. Table V shows a trade-off governed by the receding horizon length (H): a short horizon ($H = 1$) yields the lowest collision risk (0.62%) but more aggressive motion (3.000 rad/s), while longer horizons smooth the motion but increase collision risk (up to 4.83% at $H = 100$) due to accumulated mismatch between prediction and rapidly updated observations. Figure 4 confirms successful avoidance and recovery in the presence of human-induced disturbances.

4) *Comparative Analysis*: Table VI benchmarks our method against representative planners. The proposed method achieves a favorable balance between trajectory length (16.758 rad) and runtime (161.117 ms), while maintaining low collision risk. Compared with optimization baselines such as CHOMP and STOMP, it produces shorter trajectories with substantially lower computation time, demonstrating the benefit of fast, differentiable C-space distance/gradient queries.

V. CONCLUSIONS

Experiments show that CSSDF-Net enables effective safety-constrained planning and control with real-time dis-



(a) Obstacle enters affected region

(b) Obstacle leaves affected region

(c) Manipulator reaches the goal

Fig. 4: Dynamic obstacle avoidance sequence for the 7-DoF manipulator.

TABLE IV: Trajectory planning performance for the 7-DoF manipulator

Methods	Metrics		
	CR(%)↓	TL↓	AT(ms)↓
Sampling	0.274	34.279	8.846
Sampling+Non-safe Optimization	15.066	17.898	31.738
Sampling+Safe Optimization	0.561	18.054	171.117

TABLE V: Quantitative analysis of MPC online control for the 7-DoF manipulator

Receding Horizon Length	Metrics		
	CR (%)↓	MCI (rad/s)↓	CF(Hz)↑
$H = 1$	0.620	3.000	280.275
$H = 10$	3.440	2.001	204.230
$H = 50$	3.210	2.001	56.425
$H = 100$	4.830	2.001	39.098

tance/gradient queries. In the 2-DoF planar setting, safe trajectory optimization achieves 0% collision risk (AT = 130.48 ms), and for the 7-DoF manipulator GPU distance+gradient inference remains fast even at large query scales (e.g., 4.302 ms at 10^4 points). These results indicate that the learned C-space distance field provides stable gradients that are directly usable in trajectory optimization and MPC.

Beyond performance, this work advocates a unified and differentiable notion of safety modeled directly in configuration space, covering both self-collision and environment collision within a single geometric representation. By avoiding workspace-to-C-space projections and leveraging a spatial-hashing-based data pipeline, CSSDF-Net targets deployment in unseen scenes without environment-specific retraining, making it a practical backend for vision-guided motion planning in unstructured and dynamic environments.

For future work. Although online updates are supported through repeated point-cloud queries, the model is not explicitly spatiotemporal; extending the formulation toward 4D (space-time) representations is a natural direction for richer dynamic-obstacle modeling. In addition, robustness to sensing noise, partial observability, and calibration errors should be strengthened via uncertainty-aware training and more conservative safety margins. Finally, scaling to dense scenes and multi-agent settings will require more efficient point selection/aggregation and principled coordination mechanisms that couple multiple robots under shared safety constraints.

TABLE VI: Comparative trajectory planning performance for the 7-DoF manipulator

Algorithms	Metrics		
	CR(%)↓	TL↓	AT (ms)↓
RRT-Connect [24]	0.274	34.279	8.846
BiEST [25]	0.256	51.036	7.715
LazyPRM [26]	0.258	8.903	422.712
KPIECE [27]	0.558	89.549	42.256
CHOMP [28]	0.236	31.492	641.569
STOMP [29]	0.312	26.792	796.784
TrajOpt [30]	0.296	23.594	191.232
RRT* [31]	0.342	5.858	501.234
EST [25]	0.997	29.488	8.1041
PDST [32]	1.278	18.677	40.621
InformedRRT* [33]	0.242	5.754	501.454
RRT [3]	1.233	19.510	7.903
Proposed Method	0.561	16.758	161.117

REFERENCES

- [1] Y. Li, X. Chi, A. Razmjoo, and S. Calinon, "Configuration space distance fields for manipulation planning," *ArXiv*, vol. abs/2406.01137, 2024.
- [2] L. Kavraki, P. Svestka, J.-C. Latombe, and M. Overmars, "Probabilistic roadmaps for path planning in high-dimensional configuration spaces," *IEEE Trans. Robot. Automat.*, vol. 12, no. 4, pp. 566–580, 1996.
- [3] S. M. LaValle, "Rapidly-exploring random trees: a new tool for path planning," *The annual research report*, 1998.
- [4] F. Gao and S. Shen, "Online quadrotor trajectory generation and autonomous navigation on point clouds," in *2016 IEEE International Symposium on Safety, Security, and Rescue Robotics (SSRR)*, 2016, pp. 139–146.
- [5] F. Gao, W. Wu, Y. Lin, and S. Shen, "Online safe trajectory generation for quadrotors using fast marching method and bernstein basis polynomial," in *2018 IEEE International Conference on Robotics and Automation (ICRA)*, 2018, pp. 344–351.
- [6] F. Gao, W. Wu, W. Gao, and S. Shen, "Flying on point clouds: Online trajectory generation and autonomous navigation for quadrotors in cluttered environments," *Journal of Field Robotics*, vol. 36, pp. 710–733, 2018.
- [7] S. Liu, M. Watterson, K. Mohta, K. Sun, S. Bhattacharya, C. J. Taylor, and V. Kumar, "Planning dynamically feasible trajectories for quadrotors using safe flight corridors in 3-d complex environments," *IEEE Robotics and Automation Letters*, vol. 2, no. 3, pp. 1688–1695, 2017.
- [8] R. Deits and R. Tedrake, "Computing large convex regions of obstacle-free space through semidefinite programming," in *Algorithmic Foundations of Robotics XI: Selected Contributions of the Eleventh International Workshop on the Algorithmic Foundations of Robotics*. Springer, 2015, pp. 109–124.
- [9] H. Dai, A. Amice, P. Werner, A. Zhang, and R. Tedrake, "Certified polyhedral decompositions of collision-free configuration space," *The International Journal of Robotics Research*, vol. 43, no. 9, pp. 1322–1341, 2024.
- [10] M. Petersen and R. Tedrake, "Growing convex collision-free regions in configuration space using nonlinear programming," *arXiv preprint arXiv:2303.14737*, 2023.

- [11] P. Werner, R. Cheng, T. Stewart, R. Tedrake, and D. Rus, "Superfast configuration-space convex set computation on gpus for online motion planning," *ArXiv*, vol. abs/2504.10783, 2025.
- [12] S. Cameron, "Enhancing GJK: Computing minimum and penetration distances between convex polyhedra," in *Proceedings of international conference on robotics and automation*, vol. 4. IEEE, 1997, pp. 3112–3117.
- [13] J. Pan, S. Chitta, and D. Manocha, "Fcl: A general purpose library for collision and proximity queries," in *2012 IEEE International Conference on Robotics and Automation*, 2012, pp. 3859–3866.
- [14] E. Coumans, "Bullet physics simulation," *ACM SIGGRAPH 2015 Courses*, 2015.
- [15] H. Oleynikova, M. Burri, Z. Taylor, J. Nieto, R. Siegwart, and E. Galceran, "Continuous-time trajectory optimization for online uav replanning," in *2016 IEEE/RSJ international conference on intelligent robots and systems (IROS)*. IEEE, 2016, pp. 5332–5339.
- [16] F. Gao, Y. Lin, and S. Shen, "Gradient-based online safe trajectory generation for quadrotor flight in complex environments," in *2017 IEEE/RSJ international conference on intelligent robots and systems (IROS)*. IEEE, 2017, pp. 3681–3688.
- [17] V. Vasilopoulos, S. Garg, P. Piacenza, J. Huh, and V. Isler. RAMP: Hierarchical reactive motion planning for manipulation tasks using implicit signed distance functions.
- [18] M. Koptev, N. Figueroa, and A. Billard, "Real-time self-collision avoidance in joint space for humanoid robots," vol. 6, no. 2, pp. 1240–1247.
- [19] Y. Li, X. Chi, A. Razmjoo, and S. Calinon, "Configuration space distance fields for manipulation planning," *arXiv preprint arXiv:2406.01137*, 2024.
- [20] N. D. Ratliff, J. Issac, D. Kappler, S. Birchfield, and D. Fox, "Riemannian motion policies," *arXiv preprint arXiv:1801.02854*, 2018.
- [21] K. Van Wyk, M. Xie, A. Li, M. A. Rana, B. Babich, B. Peele, Q. Wan, I. Akinola, B. Sundaralingam, D. Fox, *et al.*, "Geometric fabrics: Generalizing classical mechanics to capture the physics of behavior," *IEEE Robotics and Automation Letters*, vol. 7, no. 2, pp. 3202–3209, 2022.
- [22] I. Loshchilov and F. Hutter, "Decoupled weight decay regularization," in *International Conference on Learning Representations*, 2017.
- [23] Y. Malkov and D. A. Yashunin, "Efficient and robust approximate nearest neighbor search using hierarchical navigable small world graphs," *IEEE Transactions on Pattern Analysis and Machine Intelligence*, vol. 42, pp. 824–836, 2016.
- [24] J. Kuffner and S. LaValle, "RRT-connect: An efficient approach to single-query path planning," in *Proceedings 2000 ICRA. Millennium Conference. IEEE International Conference on Robotics and Automation. Symposia Proceedings (Cat. No.00CH37065)*, vol. 2, 2000, pp. 995–1001 vol.2.
- [25] D. Hsu, J.-C. Latombe, and R. Motwani, "Path planning in expansive configuration spaces," *Proceedings of International Conference on Robotics and Automation*, vol. 3, pp. 2719–2726 vol.3, 1997.
- [26] R. Bohlin and L. Kavraki, "Path planning using lazy prm," in *Proceedings 2000 ICRA. Millennium Conference. IEEE International Conference on Robotics and Automation. Symposia Proceedings (Cat. No.00CH37065)*, vol. 1, 2000, pp. 521–528 vol.1.
- [27] I. A. Sucan and L. E. Kavraki, "A sampling-based tree planner for systems with complex dynamics," *IEEE Transactions on Robotics*, vol. 28, no. 1, pp. 116–131, 2012.
- [28] N. Ratliff, M. Zucker, J. A. Bagnell, and S. Srinivasa, "Chomp: Gradient optimization techniques for efficient motion planning," in *2009 IEEE International Conference on Robotics and Automation*, 2009, pp. 489–494.
- [29] M. Kalakrishnan, S. Chitta, E. Theodorou, P. Pastor, and S. Schaal, "Stomp: Stochastic trajectory optimization for motion planning," in *2011 IEEE International Conference on Robotics and Automation*, 2011, pp. 4569–4574.
- [30] J. Schulman, Y. Duan, J. Ho, A. X. Lee, I. Awwal, H. Bradlow, J. Pan, S. Patil, K. Goldberg, and P. Abbeel, "Motion planning with sequential convex optimization and convex collision checking," *The International Journal of Robotics Research*, vol. 33, pp. 1251 – 1270, 2014.
- [31] S. Karaman and E. Frazzoli, "Sampling-based algorithms for optimal motion planning," *The International Journal of Robotics Research*, vol. 30, pp. 846 – 894, 2011.
- [32] A. M. Ladd and L. E. Kavraki, "Motion planning in the presence of drift, underactuation and discrete system changes." in *Robotics: Science and systems*, vol. 1. Boston, MA, 2005, pp. 233–240.
- [33] J. D. Gammell, S. S. Srinivasa, and T. D. Barfoot, "Informed rrt*: Optimal sampling-based path planning focused via direct sampling of an admissible ellipsoidal heuristic," in *2014 IEEE/RSJ International Conference on Intelligent Robots and Systems*, 2014, pp. 2997–3004.